Journal of ELECTRONIC MATERIALS, Vol. 46, No. 7, 2017
DOI: 10.1007/s11664-017-5374-3
© 2017 The Minerals, Metals & Materials Society

CrossMark

Influence of SnO_2 Nanoparticles Addition on Microstructure, Thermal Analysis, and Interfacial IMC Growth of Sn1.0Ag0.7Cu Solder

REN SUN,[1] YANWEI SUI,[1,2] JIQIU QI,[1] FUXIANG WEI,[1] YEZENG HE,[1] XIAO CHEN,[1] QINGKUN MENG,[1] and ZHI SUN[1]

1.—School of Material Science and Engineering, China University of Mining and Technology, Xuzhou 221116, China. 2.—e-mail: wyds123456@outlook.com

A new lead-free Sn-1.0Ag-0.7Cu-xSnO_2 composite solder was smelted in a vacuum arc furnace at 900°C for 30 min. This paper investigated the influence of SnO_2 nanoparticles on the microstructure, melting properties and growth of interfacial intermetallic compounds (IMCs) at the interface between Cu and the composite solder during isothermal aging. The results indicated that SnO_2 particles effectively refined the β-Sn grains and reduced the size of Cu_6Sn_5. The thermal analysis data showed that nano-sized SnO_2 decreased the pasty range and melting temperature. In addition, the additional nanoparticles reduced the diffusion coefficient and impeded the growth of intermetallic compounds during soldering and aging. The effect of nanoparticles on solder is closely associated with the added amount of nano-SnO_2 particles. When the SnO_2 concentration was 1.0 wt.%, the composite solder possessed an excellent microstructure, suitable melting properties and obvious inhibition effect on the interfacial IMCs. However, excessive addition of SnO_2 particles in the solder alloys decreased the inhibition effect of the interfacial IMCs.

Key words: Composite solder, microstructure, interfacial intermetallic compounds growth, SnO_2 nanoparticles addition

INTRODUCTION

Sn-Pb solders have been widely utilized in the electronics industry in the past few decades due to their low melting point, desirable ability to wet substrates and superior mechanical properties. However, the existence of Pb in solders leads to serious environmental and health issues.[1,2] Considering these problems, researchers have made extensive efforts to find viable lead-free solders for microelectronics assembly.[3] Among series of lead-free solders, the Sn-Ag-Cu lead-free solders including Sn-3.0Ag-0.7Cu and Sn-3.8Ag-0.7Cu have been considered as the most promising alternatives for toxic Sn-Pb solders because of their superior mechanical properties and soldering performance.[4] Nowadays, electronic devices have become thinner, lighter, and smaller which has encouraged the development of high density and miniaturization for the electronics packages industry. However, lead-free solders face great challenges due to their coarse β-Sn grains, large brittle intermetallics and higher growth rate of interfacial intermetallic compounds (IMCs) between the solder and the substrate.[5–7] The fast growth rate and excessive thickness of interfacial IMCs exert a detrimental influence on the long-term reliability of solder joints. Moreover, the high Ag content in lead-free solders such as Sn-3.8Ag-0.7Cu and Sn-4.0Ag-0.5Cu leads to the precipitation of the brittle Ag_3Sn phase in the solder matrix, which may reduce the reliability of solder joints and increase cost.[8,9] Compared with the widely used Sn-3.0Ag-0.5Cu solder, the low-Ag Sn-Ag-Cu (SAC) solder has recently received increased attention due to its lower cost and thinner brittle Ag_3Sn IMCs.[10] However, with reducing Ag

(Received August 24, 2016; accepted February 10, 2017; published online February 24, 2017)

content, the solders show a rise in melting points, and a deterioration of wettability and strength. These defects restrict the application of low-Ag solder alloys in the microelectronics industries.[11]

In order to improve the reliability and refine the microstructure of lead-free solders, nanometer-sized oxides, intermetallic, or ceramic particles are used as reinforcement in solder matrix to fabricate composite solders. The nanoparticles can suppress the grain growth and assist in forming smaller intermetallic compounds because of their smaller size, larger surface area and higher surface energy.[12,13] Many researchers have investigated the effect of adding nanoparticles to solder alloys. El-Daly et al.[14] reported that SiC nanoparticles were effective in refining the microstructure of the composite Sn3.0Ag0.7Cu-0.7%SiC solder, increasing the strength and elastic modulus. Shen et al.[15] added ZrO_2 nanoparticles to Sn-3.5Ag solder and found that the growth of Ag_3Sn was suppressed. Grain et al.[16] also investigated the addition of ZrO_2 nanoparticles to Sn-3.0Ag-0.5Cu solder alloy. The results showed that 1.0 wt.% nano-ZrO_2 decreased the formation of the IMCs layer and enhanced the strength of the solder joint, while the melting point was slightly increased. Tang et al.[17] studied the Sn-3.0Ag-0.5Cu-xTiO_2 composite solders and pointed out that the size and spacing between Ag_3Sn grains significantly decreased. Gu et al.[18] added Fe_2O_3 nanoparticles into SnAgCu solder to investigate the influence on the IMC layer. The results indicated that the Fe_2O_3 nanoparticles ameliorated the wettability of the solder, inhibiting the growth rate of the IMC. Zhang et al.[19] demonstrated that nano-La_2O_3 improved the reliability of solder joints because of the reduction of the diffusion coefficient and activation energy of the IMCs layer.

These results show that reinforcement particles are effective in improving the properties of solders. However, the influences of SnO_2 nanoparticles on the properties of low-Ag lead-free Sn-1.0Ag-0.7Cu solder have not so far been researched. Compared with other particles, nano-SnO_2 has a density close to that of SAC solder, a higher hardness than solder matrix and a lower cost than other nanoparticles such as TiO_2, SiC or ZrO_2.[20] In this study, a lead-free Sn-1.0Ag-0.7Cu composite solder mixed with SnO_2 nanoparticles was prepared by a mechanically dispersing method. This paper studied the effects of SnO_2 on the microstructure and melting properties of Sn-1.0Ag-0.7Cu lead-free solders. Meanwhile, the diffusion coefficient at the interface was calculated and the IMCs growth between the solders and the Cu substrates were discussed under isothermal aging.

EXPERIMENTAL

The Preparation of Nano-Composite Solders

The nano-composite solder alloys were prepared using the smelting method. The particles of tin (99.99%), silver (99.99%) and copper (99.99%) with a size about 3 mm were obtained from Beijing Purui New Materials Technology. Nano-SnO_2 particles (99.99%) with a size about 50–70 nm were obtained from Aladdin Industrial. Pure metals and nano-SnO_2 particles were put in a Cu crucible, and then melted in a vacuum arc furnace at about 900°C for 30 min to prepare Sn-Ag-Cu-xSnO_2 (x = 0 wt.%, 0.3 wt.%, 0.7 wt.%, 1.0 wt.%, and 1.3 wt.%) composite solders. The vacuum degree was 5 Pa $\times 10^{-3}$ Pa to prevent oxidation. Finally, the alloys were cast with a water-cooling condition, so as to achieve a fine microstructure. In order to obtain a uniform composition within the ingots, the metal alloy was re-melted four times in the vacuum arc furnace. Meanwhile, an electromagnetic stirrer was applied to ensure the distribution of SnO_2 nanoparticles during vacuum arc melting. Figure 1 shows the scanning electron microscope (SEM) images of initial SnO_2 nanoparticles. The SnO_2 particles exhibit a spherical shape with a size of 50–70 nm.

Microstructure Investigation

For metallographic observation, the specimens were ground with sandpaper, polished with 0.05-μm Al_2O_3 powers, and then etched with 10% HNO_3 and 90% ethyl alcohol solution. The microstructure were observed by optical microscopy and SEM with the backscattered electron. X-ray diffraction (XRD) was adopted to determine the phase composition of the specimens.

Differential Scanning Calorimeter

A differential scanning calorimeter (DSC) was used to investigate the melting properties of Sn-1.0Ag-0.7Cu (SAC107)-xSnO_2 composite solders. Approximately 5 mg of each solder was heated at a rate of 10°C/min in a nitrogen atmosphere.

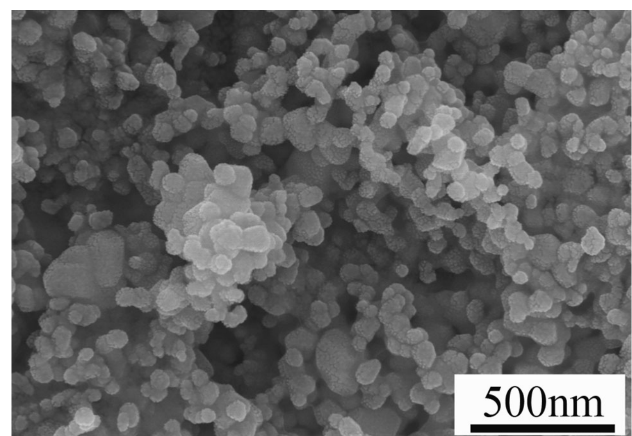

Fig. 1. SEM image of SnO_2 nanoparticles.

Interfacial IMC Layers Growth Under Isothermal Aging Condition

The Cu substrate (99.99%) was ground smooth with SiC paper, and was cut with a wire-cutting machine into rectangular blocks (20 mm × 20 mm × 1 mm). The solder joints between mmSn-1.0Ag-0.7Cu-xSnO_2 and mmCu substrate were heated to 300°C for 8 min in a resistance furnace. In this process, the solder was covered by Rosin mildly activated flux to avoid oxidation. Then, the solder joints were subject to an isothermal aging test. The aging temperature was 150°C and the aging times were 100 h, 200 h, and 300 h.

In order to observe the interface, cross-section specimens were mounted in Bakelite and prepared by metallographic procedures. Finally, the interfacial morphologies at the solder alloy/substrates interface were observed by using SEM. The thickness of the IMCs layer was the quotient which was obtained from the area of the IMCs layer divided by its length and the area of the IMCs layer was measured by Auto CAD technology software.

RESULTS AND DISCUSSION

Figure 2 shows the XRD patterns of SnO_2 nanoparticles and lead-free composite solders. Figure 2a shows the tetragonal cassiterite SnO_2-type structure with no impurities existing in the XRD patterns, indicating that the particles are pure SnO_2 nanoparticles. It is obvious that β-Sn, Ag_3Sn and Cu_6Sn_5 are observed in all composite solders, which have been similarly reported by El-Daly et al.[21] There is no diffraction peak of SnO_2 in the original SAC107 solder matrix. When the added amount of nano-SnO_2 particles in solder alloy is 0.3 wt.%, the SnO_2 phase is found in the XRD spectra. This indicates that SnO_2 nanoparticles exist in the Sn-1.0Ag-0.7Cu solders.

Figure 3 shows the microstructure images of the Sn-1.0Ag-0.7Cu-xSnO_2 composite solders. The typical microstructure of the solder contains primary β-Sn phases and eutectic phases, and these eutectic phases are located in the boundary of the β-Sn phases. Figure 3 reveals that the addition of SnO_2 nanoparticles into the SAC107 solder effectively influences the microstructures of solder matrix. The microstructure of the composite solders is clearly refined with the addition of SnO_2 nanoparticles. It is noticeable that the SAC107-1.0SnO_2 solder exhibits a smaller grain size of the β-Sn phases than other composite solders.

Figure 4 shows the SEM micrographs of the composite solders. The lead-free SAC solder contains a primary β-Sn phase, a needle-like fine Ag_3Sn, a dot-like Ag_3Sn and an irregular Cu_6Sn_5 phase. It can be seen that a small percentage of SnO_2 nanoparticles can alter the irregular Cu_6Sn_5 phase. This phenomenon has not been found in previous studies. When the concentration of nano-SnO_2 is 1.0 wt.%, these Cu_6Sn_5 phases achieve the best grain refinement effect as shown in Fig. 4d. However, with excessive addition of nanoparticles, the length of Cu_6Sn_5 has a tendency to increase in the solder matrix.

This suppression effect of the SnO_2 nanoparticles is similar to those reported in other studies.[22–24] In solder alloys, the SnO_2 nanoparticles can provide many heterogeneous nucleation sites to refine the microstructure.[21] Also, the nanoparticles can pin at the grain boundary to impede the grain growth.[25] However, excessive nanoparticles increase the possibility of an agglomeration phenomenon. The agglomerated nanoparticles reduce the amount of nanoparticles, which can decrease the nucleation density and finally weaken the suppression effect. The SnO_2 particles on the surface of the SAC107-1.3SnO_2 solder matrix were observed by SEM with a deep-etching metallographic technique. Figure 5

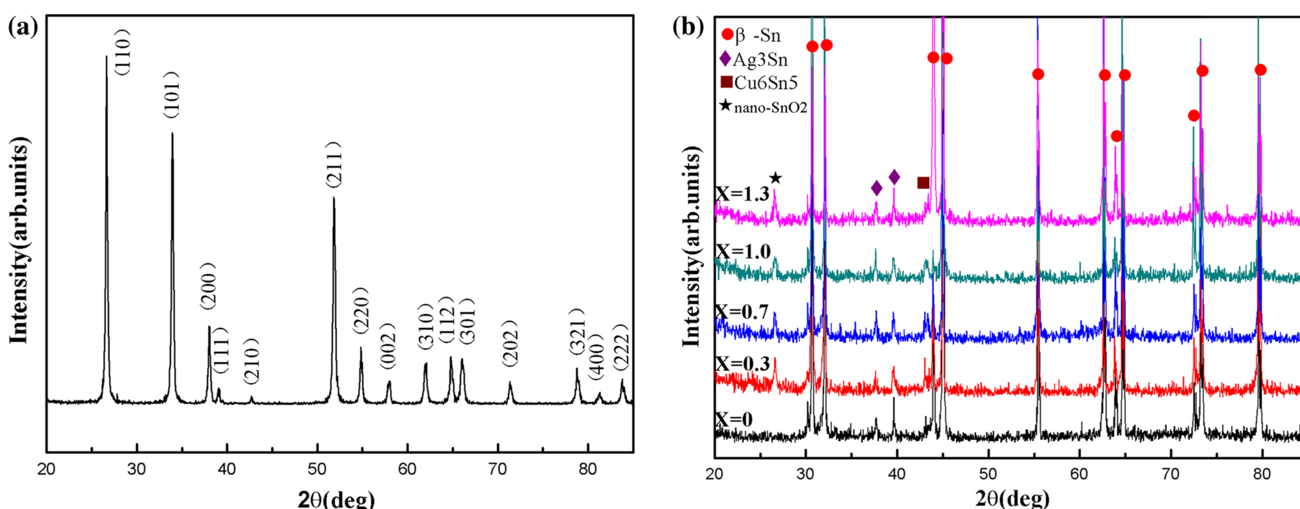

Fig. 2. (a) XRD spectrum of SnO_2 nanoparticles; (b) XRD analyses of Sn-Ag-Cu-xSnO_2 (x = 0, 0.3, 0.7, 1.0, 1.3).

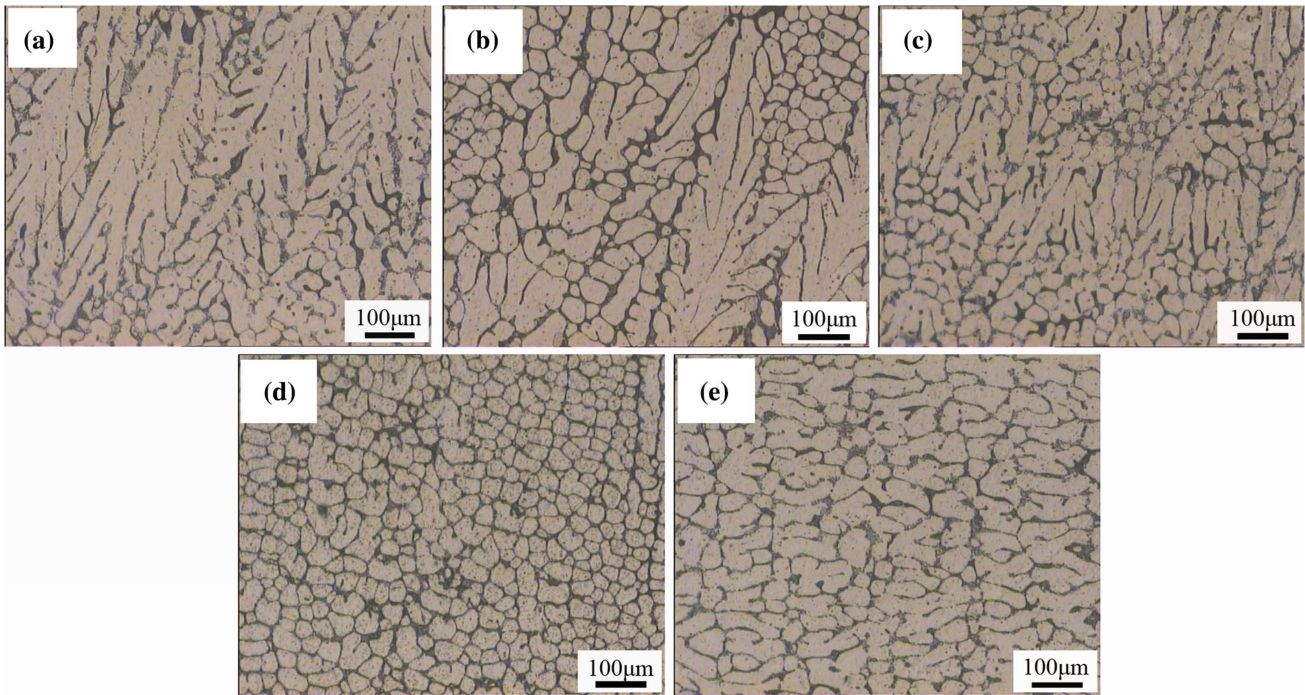

Fig. 3. Microstructure of nano-composite solders: (a) SAC107, (b) SAC107-0.3SnO_2, (c) SAC107-0.7SnO_2, (d) SAC107-1.0SnO_2, (e) SAC107-1.3SnO_2.

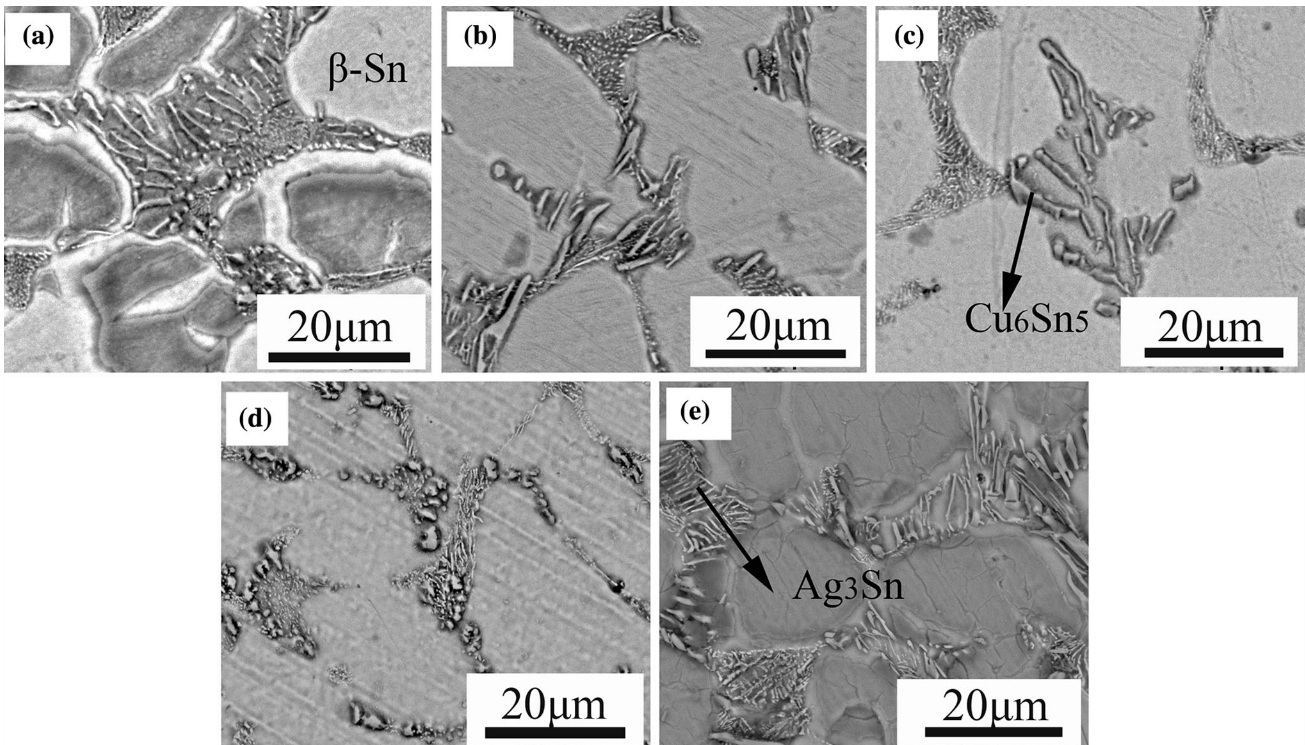

Fig. 4. SEM images of IMCs in nano-composite solder: (a) SAC107, (b) SAC107-0.3SnO_2, (c) SAC107-0.7SnO_2, (d) SAC107-1.0SnO_2, (e) SAC107-1.3SnO_2.

shows the agglomerated SnO_2 particles on the surface of the SAC107-1.3SnO_2 solder matrix. The nano-SnO_2 particles agglomerated into larger size particles with a size of about 130 nm.

Figure 6 shows the DSC curves of the solder alloys mixed with different weight percents of SnO_2 nanoparticles. During heating, the melting temperature and the solidus temperature of the composite

solders change slightly from 224.3°C to 222.5°C and from 219.2°C to 217.4°C with the addition 1.0 wt.% SnO_2 nanoparticles, respectively. The decline in the melting temperature and solidus temperature is less than 2°C for the composite solders. These changes can be ignored in electrical packaging. Generally, the melting property is an inherent physical property.[26] Therefore, the addition of nanoparticles has little impact on the solidus temperature and melting temperature. The results are similar to previous reports for SAC composite solders.[27,28]

Table I shows the liquids temperature (T_{end}), solidus temperature (T_{onset}) and pasty range. As seen in Table I, the pasty range of SAC107, SAC107-0.3SnO_2, SAC107-0.7SnO_2, SAC107-1.0SnO_2, and SAC107-1.3SnO_2 solders is about 11.6°C, 11.5°C, 11.4°C, 11°C, and 10.9°C, respectively. The addition of nano-SnO_2 particles has resulted in a slight decrease of pasty range from 11.6°C to 11°C. It is found that the pasty range of SAC107-1.0SnO_2 is less than 11.5°C of the Sn-Pb solder.[21] According to El-Daly,[29] the larger pasty range may lead to hot tearing contraction and fillet lifting phenomena. These problems will weaken the reliability of the solder joint. For these reasons, the composite solders with SnO_2 nanoparticles have exhibited better reliability than SAC107 alloy solder.

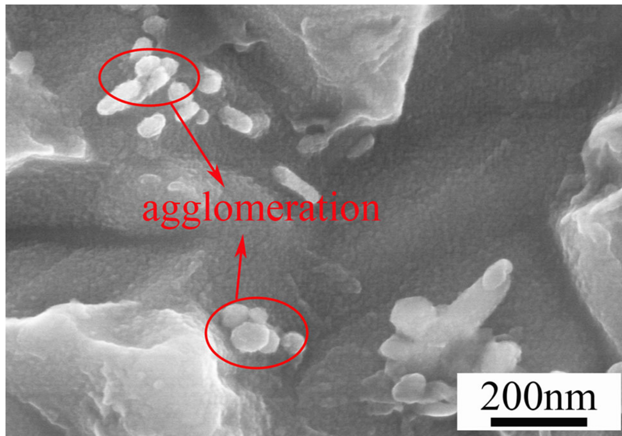

Fig. 5. SnO_2 particles on the surface of the SAC107-1.3SnO_2 solder matrix

In addition, the undercooling measured from the DSC curves for solder alloys is shown in Table II. It is notable that, with the increase of nanoparticle content, the undercooling increases from 28.9°C to 32.9°C. High undercooling may provoke grain growth in the as-cast microstructure. Although the undercooling of composite solder is higher, its microstructure is finer than the original solder alloy. This indicates that the second phases play an important role in refining the grains. These additional particles can provide many heterogeneous nucleation sites for the nucleation of primary β-Sn phases and eutectic structures.[14]

Figure 7 shows the microstructural morphology of the IMC layer between the solder and the Cu joint aged at 150°C for different times (0 h, 100 h, 200 h, and 300 h). For all the samples, the uneven scallop-shaped Cu_6Sn_5 IMC layer form at the solder/Cu interface during the soldering reaction. With the aging time increasing, the morphology of interfacial IMC layer gradually transforms from the uneven scallop-shaped to the planar-type in the Sn-1.0Ag-0.7Cu composite solder joints. After aging for 100 h, two kinds of interfacial IMCs can be observed in the soldered joints.

Figure 8 shows the composition of IMCs between SAC107 solders and the Cu substrate after aging for 100 h. From the energy-dispersive x-ray spectroscopy (EDS) results (Fig. 8b and Table III), it can be seen that the interfacial IMCs consist of Cu and Sn atoms. According to the elemental analysis, the IMCs layer in part 1 and part 2 is identified as Cu_6Sn_5 and Cu_3Sn, respectively. In the soldering process, the Sn

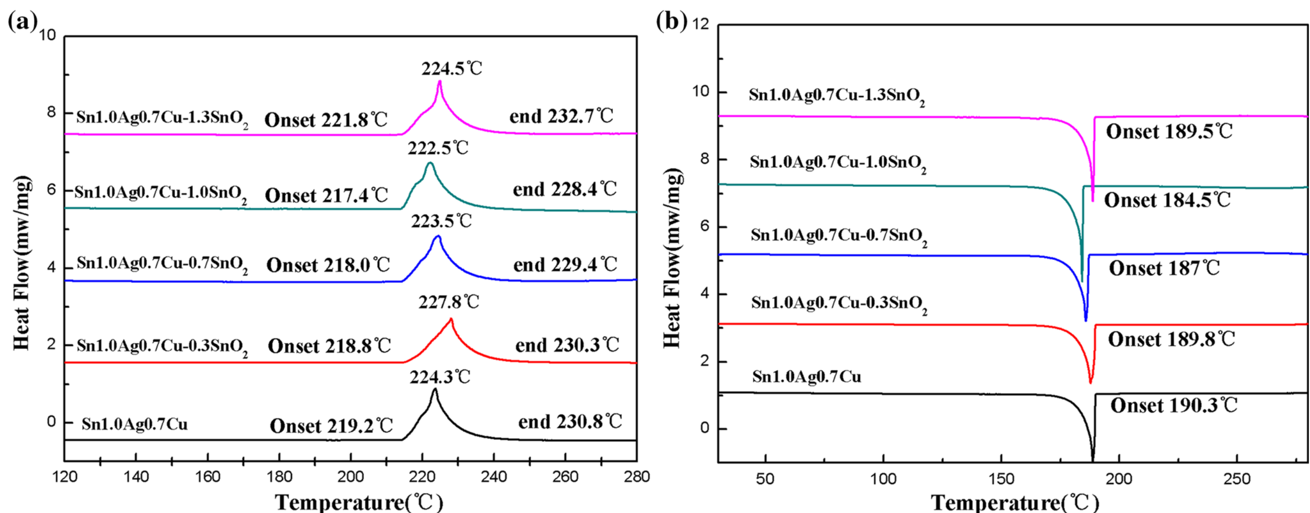

Fig. 6. Melting properties of the solders: (a) DSC heating curves (b) DSC cooling curves.

Table I. Solidus temperature (T_{onset}), liquidus temperature (T_{end}), pasty range and melting temperature for solder alloys during the heating curve

Alloy	T_{onset} (°C)	T_{end} (°C)	Pasty range ($T_{end}-T_{onset}$) (°C)	Melting temperature (°C)
SAC107	219.2	230.8	11.6	224.3
SAC107-0.3SnO_2	218.8	230.3	11.5	227.8
SAC107-0.7SnO_2	218.0	229.4	11.4	223.5
SAC107-1.0SnO_2	217.4	228.4	11	222.5
SAC107-1.3SnO_2	221.8	232.7	10.9	224.5

Table II. Undercooling range of solder alloys

Alloy	T_{onset} heating (°C)	T_{onset} cooling (°C)	Undercooling (°C)
SAC107	219.2	190.3	28.9
SAC107-0.3SnO_2	218.8	189.8	29
SAC107-0.7SnO_2	218.0	187.0	31
SAC107-1.0SnO_2	217.4	184.5	32.9
SAC107-1.3SnO_2	221.8	189.5	32.3

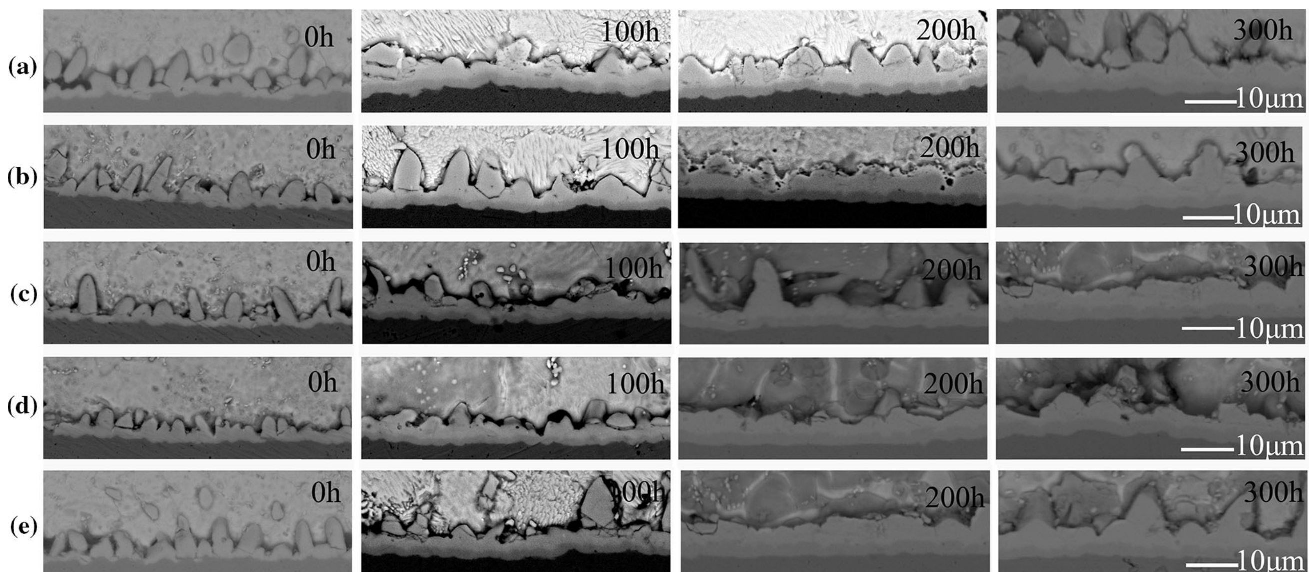

Fig. 7. Cross-section images of the SAC107-xSnO_2 composite solder and Cu substrate aged at 150°C for 100 h, 200 h, 300 h: (a) SAC107, (b) SAC107-0.3SnO_2, (c) SAC107-0.7SnO_2, (d) SAC107-1.0SnO_2, (e) SAC107-1.3SnO_2.

elements react with the Cu substrate to form Cu_6Sn_5 phases. Then, the interfacial IMCs begin to grow in the aging environment. After aging for 100 h, the Cu_3Sn phase can be detected in the interfacial IMCs layer.

Figure 9 reveals the thicknesses of the IMCs at the interface with different aging times. The interfacial thickness of the Sn1.0Ag0.7Cu-xSnO_2/Cu solder joint with different aging times was calculated to discover the influence of SnO_2 nanoparticles on the growth of interfacial IMCs. After soldering or aging, the interfacial thickness of the composite solders is thinner than that of SAC107 solder under the same conditions. When the additive amount of nano-SnO_2 is 1.0 wt.%, the minimum thickness can be achieved at any aging time. The thickness of the IMCs layer between SAC107-1.0SnO_2 and the Cu substrate improves from 3.68 μm to 6.29 μm with the increase of aging time. The results reveal that nano-SnO_2 inhibits the growth of the interfacial IMCs layer. This phenomenon is consistent with other researchers' results.[30]

Figure 10 shows the relationship between IMCs thickness and the square of aging time ($h^{1/2}$). This relationship reveals that the growth of interfacial IMC is controlled by a diffusion mechanism.[31]

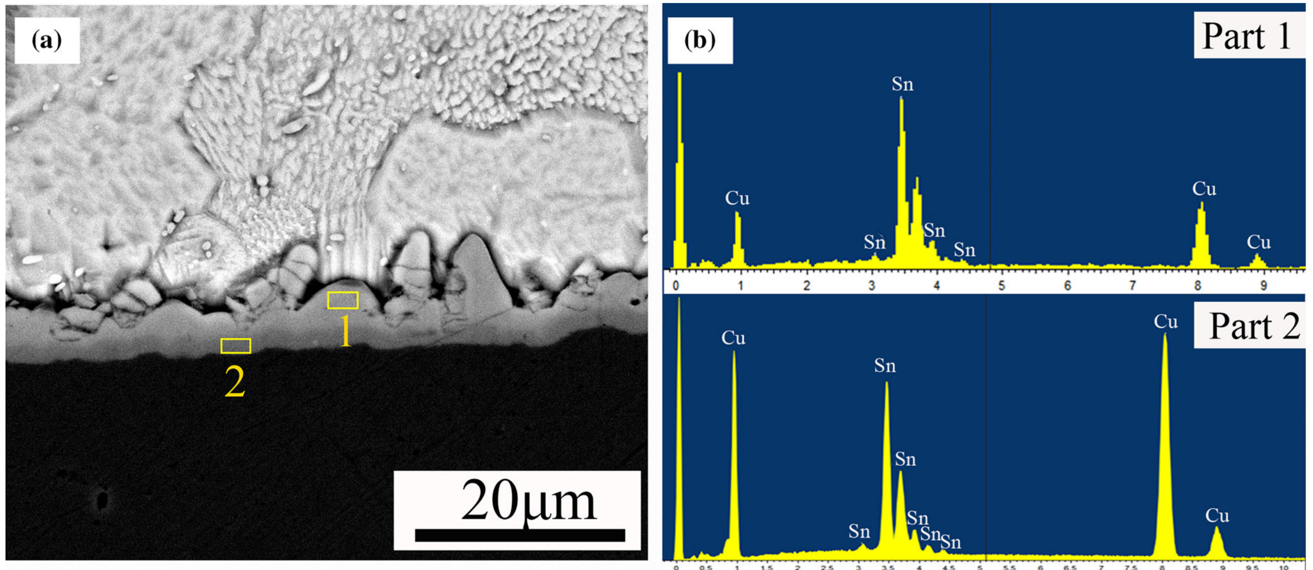

Fig. 8. (a) SEM image of the IMC layer at the Sn1.0Ag0.7Cu solder/Cu interface aged at 100 h; (b) EDS analysis of the different parts of IMC layers at the solder/Cu interface.

Table III. SEM-EDS measurements of the interfacial IMC layer at the solder/Cu interface

	Cu (at.%)	Sn (at.%)	Phase
Part 1	51.42	48.58	Cu_6Sn_5
Part 2	71.43	28.57	Cu_3Sn

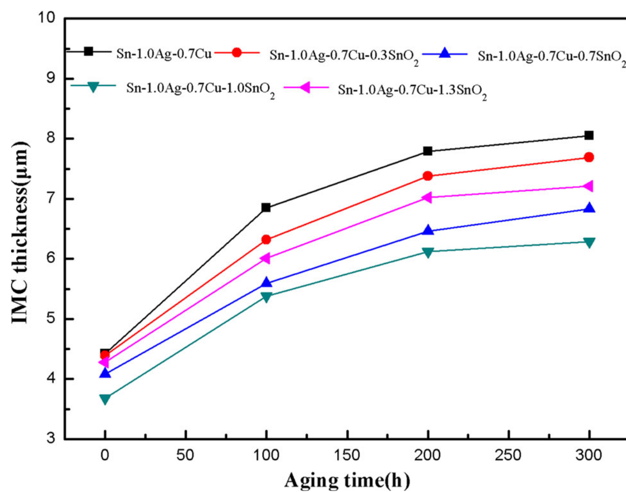

Fig. 9. Average thickness of the Sn1.0Ag0.7Cu-xSnO_2 solder/Cu interface for different aging times.

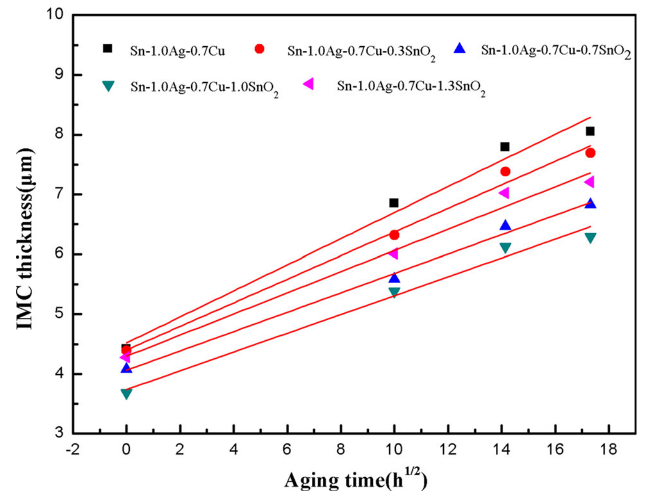

Fig. 10. Relationship between the thickness of the IMC layer and the square of aging time.

Therefore, the thickness of the interfacial IMCs layer can be expressed as.

$$X_t = X_0 + \sqrt{Dt} \quad (1)$$

where X_t is the thickness of IMCs at isothermal aging time t, X_0 is the initial thickness after soldering. and D is the diffusion coefficient ($\mu m^2/h$).

The diffusion coefficients for the Sn1.0Ag0.7Cu-xSnO_2 solder were calculated according to Eq. 1. The relationship between the diffusion coefficients and the nanoparticles proportion in the solder joints is shown in Fig. 11. It can be seen that the diffusion coefficient decreases from 0.0475 $\mu m^2/h$ to 0.0247 $\mu m^2/h$ and then increases to 0.0313 $\mu m^2/h$

with the increase of nano-SnO_2 content. When the weight percentage of the SnO_2 nanoparticles is 1.0 wt.%, the diffusion coefficients are reduced by 48% compared with the Sn1.0Ag0.7Cu solder. This result proves that the appropriate content of SnO_2 nanoparticles can reduce the diffusion coefficients of the interfacial IMCs layer during isothermal aging. Therefore, the composite solder joints with a slight amount of nano-SnO_2 particles are effective in impeding the growth of the interface IMC layer, but excessive addition will weaken the inhibition effect.

The proposed explanation for the effect of SnO_2 nanoparticles on the formation and growth of the interfacial IMCs layer is attributed to the adsorption ability of nanoparticles. Considering the adsorption theory of SnO_2 nanoparticles,[32] the surface energy of a whole crystal (Cu_6Sn_5 grain) is:

$$\sum_{k} \gamma^{k}_{(c)} A_{k} = \sum_{k} \left(\gamma^{k}_{(0)} - RT \int_{0}^{c} \frac{\Gamma^{k}}{c} \mathrm{d}c \right) A_{k} \quad (2)$$

$$= \sum_{k} \gamma^{k}_{(0)} A_{k} - RT \sum_{k} A_{k} \int_{0}^{c} \frac{\Gamma^{k}}{c} \mathrm{d}c \rightarrow \min \quad (3)$$

where Γ^k is the absorption amount of nanoparticles at the crystal planes k, A_k is the area of the crystal planes k, $\gamma^{k}_{(0)}$ is the surface tension of Cu_6Sn_5 grain without adsorption, $\gamma^{k}_{(c)}$ is the surface tension of Cu_6Sn_5 grain with adsorption of nano-SnO_2 particles, c is the concentration of SnO_2 nanoparticles, R is the gas constant, and T is the absolute temperature. Gibbs tells us that the reduction of surface energy can decrease the growth velocity of IMCs grains. In Eq. 3 $\sum_k \gamma^{k}_{(0)} A_k$ and RT are assumed to be constant because they are unrelated to the content of SnO_2 nanoparticles. That is,

$$RT \sum_{k} A_{k} \int_{0}^{c} \frac{\Gamma^{k}}{c} \mathrm{d}c \rightarrow \max \quad (4)$$

This relationship implies that Eq. 4 can be maximized with a maximum amount of absorption of nanoparticles at the crystal planes. Therefore, the increasing amount of absorbed particles can generate a decrease in the surface energy of a whole crystal and reduce the growth rate of the crystal plane. This theory has been reported by some researchers to explain the effect of nanoparticles on IMC growth,[18,19] and these researchers have found that the nano-sized Fe_2O_3, La_2O_3 were absorbed on the surface of interfacial Cu_6Sn_5 grains and suppressed the growth of IMCs layer. However, some researchers have not found nanoparticles at the soldered interface, but the growth of interfacial IMC layers have still been inhibited.[15,33]

According to the equation of adsorption theory, there is no doubt that the nanoparticles absorbed on the surface of Cu_6Sn_5 grains can reduce the surface energy, so as to hinder the growth of the IMCs layer during soldering or aging: the larger the number of adsorption nanoparticles, the smaller the surface energy of the IMCs. However, when the nanoparticles are excessive, the nano-sized SnO_2 agglomerate into large-sized particles. Agglomerated nanoparticles reduce the adsorption ability due to their lower surface energy. Actually, the absorbed number of nanoparticles declines because of the agglomerated particles, which weaken the growth rate of the interface IMCs in the interface of the solder/Cu substrate. In addition, the diffusion of the Sn and Cu atoms is retarded by the nanoparticles on the surface of the interfacial IMCs which can act as an obstacle, resulting in a lower growth rate for interfacial Cu-Sn IMCs during soldering and isothermal aging.

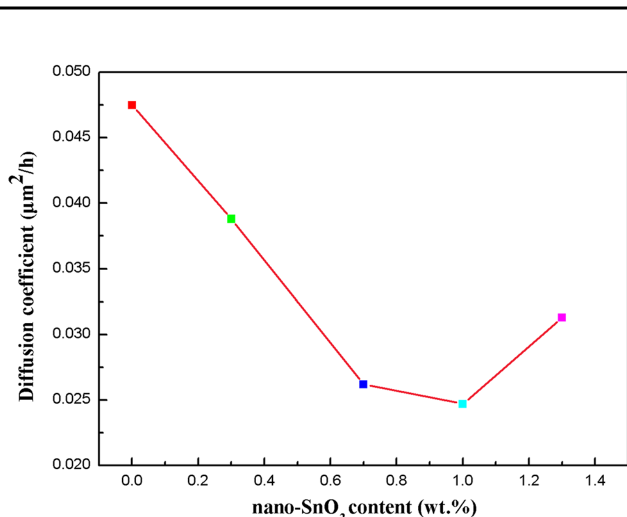

Fig. 11. Growth rates of IMC layer versus nano-SnO_2 content.

CONCLUSIONS

This study investigated the effects of nano-SnO_2 addition on the microstructure, melting properties and interfacial IMCs layer growth of Sn1.0Ag0.7Cu solder. The major conclusions are summarized as follows:

1. The addition of SnO_2 particles refined the microstructure of the SAC107 solder matrix. The addition of a slight amount of nanoparticles in SAC107 solder decreased the size of the β-Sn and Cu_6Sn_5 in the solder matrix. However, excessive addition weakens the refinement extent. The composite solder SAC107-1.0SnO_2 displayed a finer microstructure due to the heterogeneous nucleation of SnO_2 particles.
2. The nano-SnO_2 particles in the SAC107 solder decreased the melting temperature and pasty range although the undercooling was slightly increased. The decrease in melting temperature and pasty range was less than 2°C, which

indicated that the composite solder was applicable in existing soldering processes.

3. The nano-SnO_2 particles were effective in inhibiting the growth of the interfacial IMCs layer during soldering and aging. The thickness of the interfacial IMCs decreased with increasing SnO_2 content from 0.3 wt.% to 1.0 wt.%, which could be attributed to the adsorption of nanoparticles.

ACKNOWLEDGEMENT

The research was financially supported by the National Natural Science Foundation (51671214, 51601220) and Science and technology project of Jiangsu Province (BY2016026-05).

REFERENCES

1. M.M. Billah, K.M. Shorowordi, and A. Sharif, *J. Alloys Comp.* 585, 32 (2014).
2. I. Anderson, *J. Mater. Sci. Mater. Electron.* 18, 55 (2007).
3. K.S. Kim, S.H. Huh, and K. Suganuma, *J Alloys Compd.* 352, 226 (2003).
4. H. Hao, Y.W. Shi, Z.D. Xia, Y.P. Lei, and F. Gao, *J. Electron. Mater.* 37, 2 (2008).
5. L. Zhang, X.Y. Fan, Y.H. Guo, and C.W. He, *Mater. Des.* 57, 646 (2014).
6. G.Y. Li, X.D. Bi, Q. Chen, and X.Q. Shi, *J. Electron. Mater.* 40, 165 (2011).
7. S.Y. Chang, C.C. Jain, T.H. Chuang, L.P. Feng, and L.C. Tsao, *Mater. Des.* 32, 4720 (2011).
8. Y.S. Lai, P.F. Yang, and C.L. Yeh, *Microelectron. Reliab.* 46, 645 (2006).
9. D.A.A. Shnawah, S.B.M. Said, M.F.M. Sabri, I.A. Bradruddin, and F.X. Che, *Microelectron. Reliab.* 52, 2701 (2012).
10. J.E. Spinelli and A. Garcia, *J. Mater. Sci. Mater. Electron.* 25, 478 (2014).
11. J.H. Lee, A.M. Yu, J.H. Kim, M.S. Kim, and N. Kang, *Met. Mater. Int.* 14, 649 (2008).
12. G. Zeng, S.D. McDonald, Q. Gu, Y. Terada, K. Uesugi, H. Yasuda, and K. Nogita, *Acta Mater.* 83, 357 (2015).
13. T. Ishizaki, M. Usui, and Y. Yamada, *Microelectron. Reliab.* 55, 1861 (2015).
14. A.A. El-Daly, W.M. Desoky, T.A. Elmosalami, M.G. El-Shaarawy, and A.M. Abdraboh, *Mater. Des.* 65, 1196 (2015).
15. J. Shen, Y.C. Liu, Y.J. Han, Y.M. Tian, and H.X. Gao, *J. Electron. Mater.* 35, 1672 (2006).
16. A.K. Gain, Y.C. Chan, *Microelectron. Reliab.* 54, 945 (2014).
17. Y. Tang, G.Y. Li, and Y.C. Pan, *Mater. Des.* 55, 574 (2014).
18. Y. Gu, X. Zhao, Y. Li, Y. Liu, Y. Wang, and Z. Li, *J. Alloys Compd.* 627, 39 (2015).
19. L. Zhang and L.L. Gao, *J. Alloys Compd.* 635, 55 (2015).
20. P. Babaghorbani, S.M.L. Nai, and M. Gupta, *J. Mater. Sci. Mater. Electron.* 20, 571 (2009).
21. A.A. El-Daly, T.A. Elmosalami, W.M. Desoky, M.G. El-Shaarawy, and A.M. Abdraboh, *Mater. Sci. Eng. A* 618, 389 (2014).
22. L.C. Tsao, S.Y. Chang, C.I. Lee, W.H. Sun, and C.H. Huang, *Mater. Des.* 31, 4831 (2010).
23. A.K. Gain, Y.C. Chan, and W.K.C. Yung, *Microelectron. Reliab.* 51, 975 (2011).
24. J. Shen and Y.C. Chen, *J. Alloys Compd.* 477, 552 (2009).
25. X. Zhao, Y. Wen, Y. Li, Y. Liu, and Y. Wang, *J. Alloys Compd.* 662, 272 (2016).
26. X.D. Liu, Y.D. Han, H.Y. Jing, J. Wei, and L.Y. Xu, *Mater. Sci. Eng. A* 562, 25 (2013).
27. L.C. Tsao, *Mater. Sci. Eng. A* 529, 41 (2011).
28. Y. Huang, Z. Xiu, G. Wu, Y. Tian, P. He, and X. Gu, *Mate. Lett.* 169, 262 (2016).
29. A.A. El-Daly, A.E. Hammad, G.S. Al-Ganainy, and M. Ragab, *Mater. Sci. Eng. A* 608, 130 (2014).
30. S. Chellvarajoo and M.Z. Abdullah, *Mater. Des.* 90, 499 (2016).
31. P.L. Tu, Y.C. Chan, K.C. Hung, and J.K.L. Lai, *Scripta Mater.* 44, 371 (2001).
32. L.C. Tsao, *J. Alloys Compd.* 509, 8441 (2011).
33. R.W. Wu, L.C. Tsao, and R.S. Chen, *J. Mater. Sci. Mater. Electron.* 26, 1858 (2015).